



Synthesis, Characterization, Photophysical Properties of a Novel Organic Photoswitchable Dyad in Its Pristine and Hybrid Nanocomposite Forms

Gopa Mandal¹, Amrita Chakraborty², Ujjal Kumar Sur³, Balaprasad Ankamwar^{4,*},
Asish De², and Tapan Ganguly^{2,*†}

¹Department of Physics, Gobardanga Hindu College, North 24 Parganas, 743273, India

²Indian Association for the Cultivation of Science Jadavpur, Kolkata 700032, India

³Department of Chemistry, Behala College, Kolkata 700060, India

⁴Bio-Inspired Materials Science Laboratory, Department of Chemistry, University of Pune, Ganeshkhind, Pune 411007, India

Delivered by Ingenta to:

In the present paper the method of synthesis and characterization of a novel organic dyad, 3-(1-Methoxy-3,4-dihydro-naphthalen-2-yl)-1-p-chlorophenyl propenone, have been reported. In this paper our main thrust is to fabricate new hybrid nanocomposites by combining the organic dyad with different noble metals, semiconductor nanoparticle and noble metal-semiconductor core/shell nanocomposites. In this organic dyad, donor part is 1-Methoxy-3, 4-dihydro-naphthalen-2-carboxaldehyde with the acceptor *p*-chloroacetophenone. We have carried out steady state and time-resolved spectroscopic measurements on the dyad and its hybrid nanocomposite systems. Some quantum chemical calculations have also been done using Gaussian 03 software to support the experimental findings by theoretical point of view. Both from the theoretical predictions and NMR studies it reveals that in the ground state only extended (*E*-type or *trans*-type) conformation of the dyad exists whereas on photoexcitation these elongated conformers are converted into folded forms (*Z*- or *cis*-type) of the dyad, showing its photoswitchable character. Time resolved fluorescence spectroscopic (fluorescence lifetime by TCSPC method) measurements demonstrate that in chloroform medium all the organic–inorganic hybrid nanocomposites, studied in the present investigation, possess larger amount of extended conformers relative to folded ones, even in the excited singlet state. This indicates the possibility of slower energy destructive charge recombination rates relative to the rate processes associate with charge-separation within the dyad. It was found that in CHCl₃ medium, the computed charge separation rate was found to be $\sim 10^8$ s⁻¹ for the dyad alone and other hybrid nanocomposite systems. The rate is found to be faster than the energy wasting charge recombination rate $\sim 10^2$ – 10^1 s⁻¹, as observed from the transient absorption measurements for the corresponding hybrid systems. It indicates the conformational geometry has a great effect on the charge-separation and recombination rate processes. The suitability for the construction of efficient light energy conversion devices especially with Ag-Dyad nanocomposite of all the systems studied here is hinted from the observed long ion-pair lifetime.

Keywords: Hybrid Nanocomposite, Nanoparticle, Organic Dyad, Core/Shell Nanoparticle, Photoinduced Electron Transfer, Charge Recombination.

1. INTRODUCTION

Hybrid organic–inorganic nanocomposites have attracted considerable interest due to their promising optoelectronic properties.^{1–9} These hybrid systems have great

technological importance due to their potential applications in light emitting diode (LED),¹⁰ photovoltaic cells,^{11,12} organic solar cells^{13–22} etc. The function of present day solar cell can be understood by a mechanism known as ‘photoinduced electron transfer’ (PET)^{23,24} which takes place when certain photoactive materials interact with light. In the existing solar cells, PET takes place between the organic molecules and nanocrystalline inorganic phase

*Authors to whom correspondence should be addressed.

†Present address: Department of Physics, Bengal Engineering and Science University, Shibpur (BESUS), Howrah 711103, India.

to generate the charge carriers. So far, several electron acceptors have been shown to yield efficient devices in solar cell applications: conjugated polymers, fullerenes, and inorganic nanocrystals. In the class of inorganic acceptors, metal oxides are among the most studied materials. Titanium dioxide (TiO_2) has been studied in several forms: nanoparticles, porous networks, and *in situ* formation of titanium dioxide from a precursor.²⁵ The mechanism of charge separation at the organic polymer/inorganic semiconductor interface has been the subject of intense studies. Besides the application-oriented interest, fundamental studies on the coupling between Frenkel excitons on organic molecules and Wannier excitons in inorganic semiconductors have gained enormous attention.^{26–30} Non-radiative energy transfer lies at the heart of many of the optoelectronic properties of these hybrid materials.

This kind of hybrid organic–inorganic systems can provide a cost-effective alternative to conventional solar cell made of inorganic material like silicon. This is known as hybrid solar cell. As hybrid solar cell consists of both organic and inorganic materials, therefore it combines the unique properties of inorganic semiconductors with the film forming properties of the conjugated polymers. Organic materials are inexpensive, easily processable and their functionality can be tailored by molecular design and chemical synthesis. On the other hand, inorganic semiconductors can be fabricated in the form of nanoparticles by offering the advantage of having high absorption coefficients and size tunability.

Lately our research group is involved in the development of organic–inorganic nanocomposite systems by combining some organic dyads with nanoparticles^{31a} or core/shell nanoconjugates.^{31b} In the dyad systems, the donor and acceptor moieties are connected by short spacers, instead of long-chain spacers which were used by several workers in this field. The utility of short spacer was also discussed by Ganguly et al.^{31a} as well as Ohkubo et al.³² to attain long-lived charge-separated species. The short spacer has some advantages over long-chain spacer. Firstly, multi-step electron transfer process, which is responsible for tremendous loss of energy, could be avoided here. Moreover, the synthesis cost of short-chain dyad is much less than the long-chain dyads, tetrads, pentads etc. Thus it could be expected that the nanocomposites being combined with short-chain dyad may be useful for the development of efficient and low cost light energy conversion devices.

We have synthesized a short-chain organic dyad and developed several hybrid organic–inorganic nanocomposites by combining this dyad with Au, Ag, TiO_2 and Ag@TiO_2 core/shell nanoparticles. The results observed from our steady state and time-resolved spectroscopic measurements can be utilized to evaluate the capability of these hybrid nanocomposites to fight against energy crisis in the form of artificial light energy conversion devices.

2. EXPERIMENTAL DETAILS

2.1. Materials

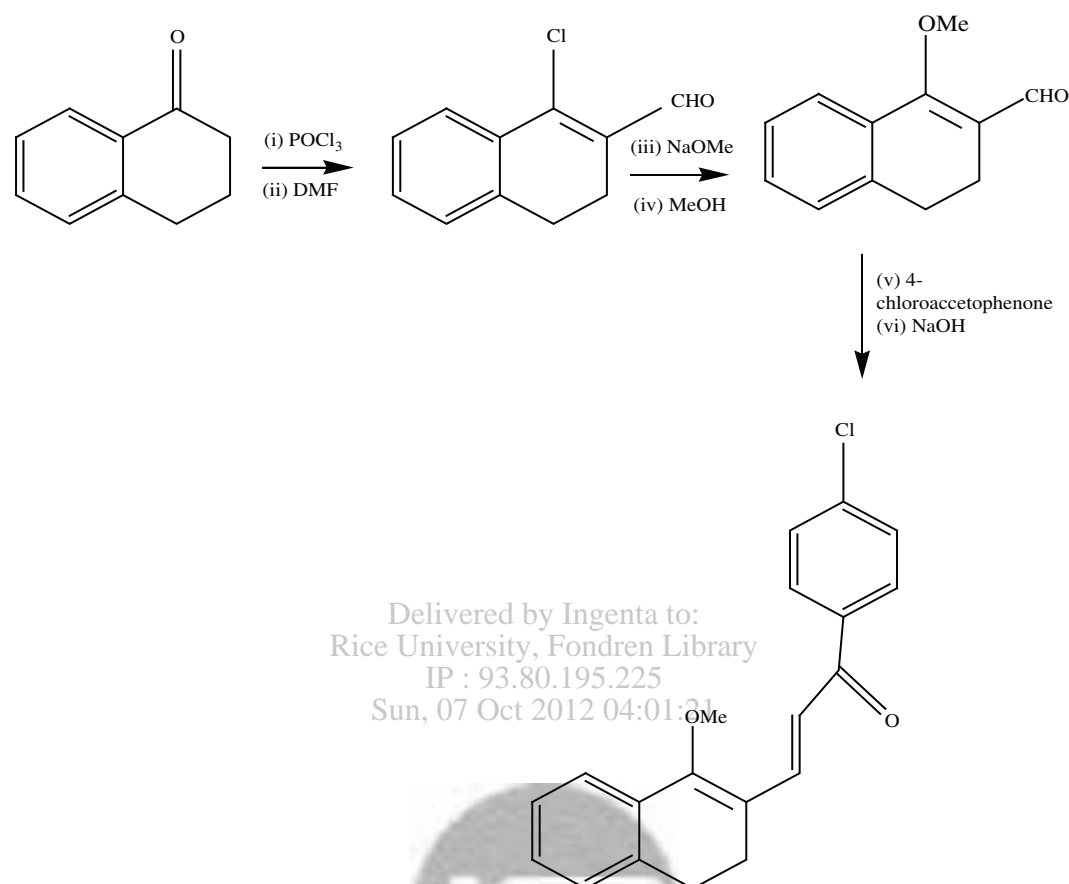
The procedure of synthesis of the donor 1-methoxy-3,4-dihydro-naphthalen-2-carboxaldehyde (1MNTCHO) and the dyad 1-(4-chloro-phenyl)-3-(1-methoxy-3,4-dihydro-naphthalen-2-yl) propenone (MNCADH) are given below and p-chloroacetophenone (PCA) is supplied from Aldrich, and used after distillation. Analytical Reagent (A.R.) grade titanium isopropoxide (TIP) (Aldrich), chloroauric acid (HAuCl_4), AgNO_3 (Merck), acetylacetone (Merck), Ammonia solution (Rankem 25%) were purchased for nanoparticle synthesis. 2-butanol (Merck), 2-propanol (Merck), acetic acid (SRL) purchased were high purity grade. The aqueous solution was prepared using Millipore water. The solvent chloroform (CHCl_3) of spectroscopic grade, purchased from Aldrich, have been distilled under vacuum according to the standard procedure and tested before use to verify the absence of any impurity emission in the concerned wavelength region. All the solutions prepared for room temperature measurements were deoxygenated by purging with an argon gas stream for about 30 minutes.

2.1.1. Synthesis and Characterization of the Organic Dyad

The dyad 1-(4-chloro-phenyl)-3-(1-methoxy-3,4-dihydro-naphthalen-2-yl) propenone (MNCADH) was synthesized from commercially available 1-tetralone in three steps as shown in the Scheme 1.

Vilsmeier-Haack reaction using freshly distilled phosphorous oxychloride and *N,N*-dimethylformamide (freshly distilled from calcium hydride), smoothly converted 1-tetralone (also freshly distilled) to 1-chloro-3,4-dihydro-naphthalene-2-carboxaldehyde. The chlorovinyl compound obtained as lightly coloured oil could be characterized from spectral data and was sufficiently pure for the next step which consisted of nucleophilic displacement of chlorine by methoxy through treatment with methanolic sodium methoxide. The resulting 1-methoxy-3,4-dihydro-naphthalene-2-carboxaldehyde (1MNTCHO) was characterized from its spectral data. Subjecting the dihydro compound to aldol condensation with 4-chloroacetophenone in the presence of sodium hydroxide resulted the target molecule, 1-(4-chloro-phenyl)-3-(1-methoxy-3,4-dihydro-naphthalen-2-yl) propenone. It was found that from the coupling constants of the olefinic protons ($J = 15$ Hz) that the dyad was present exclusively as trans geometrical isomer.

(a) *Synthesis of 1-Chloro-3,4-Dihydro-Naphthalene-2-Carboxaldehyde.* Freshly distilled phosphorous oxychloride (3 g, 5.4 ml) was added drop wise to a magnetically stirred dry DMF under anhydrous condition and external cooling (ice-salt bath) at such rate that the temperature



Scheme 1. The synthesis of the dyad 1-(4-chloro-phenyl)-3-(1-methoxy-3,4-dihydro-naphthalen-2-yl) propenone (MNCADH) from commercially available 1-tetralone.

remains between $-5\text{ }^{\circ}\text{C}$ to $0\text{ }^{\circ}\text{C}$. After the addition was complete, the reaction mixture was stirred at $0\text{ }^{\circ}\text{C}$ for 30 minutes and at $80\text{ }^{\circ}\text{C}$ for 90 minutes. After cooling to room temperature, the reaction mixture was poured into cold aqueous solution of sodium acetate (25%, 50 ml). After extraction with dichloromethane, the organic layer was washed with water and dried over sodium sulfate. Removal of solvent left reddish oil (3.16 gm) which was sufficiently pure for the next stage. The ^1H NMR spectrum in CDCl_3 , showed all the peaks characteristic of the designed product. δ (ppm) 10.29 (s, 1H, CHO) 7.79 (dd, 1H, H-8, $J = 8.1, 1.2$) 7.54–7.07 (m, 3H, H-5, H-6, H-7) 2.85–2.76 (m, 2H, H-3), 2.68–2.55 (m, 2H, H-4).

(b) *1-Methoxy-3,4-Dihydro-Naphthalene-2-Carboxaldehyde*. Sodium (0.36 gm, 1.55 mmole) was added in small portions to Mg-dry methanol (25 ml) under anhydrous condition and external cooling (ice bath). A solution of 1-chloro-3,4-dihydro-naphthalene-2-carboxaldehyde (3 g, 1.55 mmole) in Mg-dry methanol (20 ml) was added drop wise to the magnetically stirred methanolic sodium methoxide. The reaction mixture was further stirred for 30 minutes after the addition was complete followed by heating under reflux for another 1 hr. After cooling, the

reaction mixture was poured into crushed ice and acidified with dilute hydrochloric acid. After extraction with ether, the ethereal layer was washed with water and dried over sodium sulfate. Removal of solvent left a dark red oil, which indicated a mixture of the desired product and some uncharacterized impurities from the thin layer chromatography and ^1H NMR spectrum. The pure compound was isolated from column chromatography of the crude product upon elution with ethyl-acetate-petroleum ether (5:95) and was characterized from ^1H NMR spectrum.

IR (neat) 1656 cm^{-1} . ^1H NMR (CDCl_3) δ (ppm) 10.2 (s, 1H, CHO) 7.49 (dd, 1H, $J = 7.8, 1.5$, H-8), 7.303–7.105 (m, 2H, H-5, H-6, H-7) 3.83 (s, 3H, OMe) 2.71 (m, 2H, H-3), 2.46 (m, 2H, H-4).

(c) *1-(4-Chloro-Phenyl)-3-(1-Methoxy-3,4-Dihydro-Naphthalen-2-yl) Propenone*. Sodium (0.07 gm, 0.003 M) was dissolved in dry methanol under magnetic stirring in an argon atmosphere with external cooling (ice bath). To the methanolic sodium methoxide, 4-chloroacetophenone (0.464 gm, 0.003 M) was added from a syringe over 15 minutes. The reaction mixture was stirred for 45 minutes in an inert atmosphere and after this period 1-methoxy-3,4-dihydro-naphthalene-2-carbaldehyde, dissolved in dry

methanol (10 ml) was added from a syringe over 10 minutes. It was stirred further for 30 minutes followed by heating under reflux for 5 hrs. After cooling, methanol was removed under reduced pressure. The reaction mixture was extracted with ether and the etherial layer was washed with water. After drying over sodium sulfate, solvent was removed. The pure compound was isolated from the crude residue chromatographically over a silica gel column. The dyad was eluted with ethyl-acetate-petroleum ether (2:98) and was characterized spectroscopically. Yield 0.5 gm (55%).

IR γ_{\max} 1726 cm^{-1} . ^1H NMR (CDCl_3) 8.21 (d, 1H, H-3, $J = 15.6$), 7.92 (d, 1H, H-, $J = 8.4$) 7.5–7.19 (m, 8H, aromatic protons), 6.96 (d, 1H, H-2, $J = 15.3$) 3.802 (s, 3H, OMe) 2.88 (m, 2H, H-3 or H-4), 2.61 (m, 2H, H-3 or H-4).

Preparation of Ag Nanoparticles: Ag nanoparticles were synthesized from *Murraya Koenigi* leaf extract³³ as the natural source of reducing and capping biomolecules. The broth used for the reduction of Ag^+ ions to Ag^0 was prepared by taking 10 gm of thoroughly washed *Murraya koenigi* leaves in a 500 ml Erlenmeyer flasks with 40 ml of sterile distilled water and boiled it for 15 min. On cooling to room temperature, it was filtered through four fold muslin cloth and used for the synthesis of silver nanoparticles. In a typical experiment, 0.4 ml of broth was added to 9 ml of 10^{-3} M aqueous silver nitrates solution followed by addition of 0.04 ml (0.625%) ammonia solution. After shaking, it was kept for 6 hours at room temperature followed by centrifugation at 10000 rpm for 25 min. The pellets were redispersed in millipore water and centrifuged again at 10000 rpm for 10 min and collected pellets were dried in hot air oven at 65 °C for 6 hrs and characterized. The size of the Ag nanoparticle was estimated from HRTEM. Figure 1(C) shows the HRTEM images of the Ag nanoparticles. The TEM image shows that particle diameter varies in the range of 20–40 nm. The average diameter of silver nanoparticle is found to be ~30 nm.

Preparation of TiO_2 Nanoparticles: The procedure for synthesizing TiO_2 nanoparticles (Fig. 1(D)) is described in our earlier paper.^{31a}

Preparation of Ag@TiO_2 Nanoparticles: To synthesize the Ag@TiO_2 nanocomposites,^{31b} a solution containing equimolar (19.9 mM) amounts of titanium isopropoxide and acetylacetone in 2-propanol was prepared. A clear solution was formed upon mild sonication. Another solution of 8.80 mM AgNO_3 and 13.88 M H_2O in DMF was prepared. A 40 ml sample of the first solution and 20 ml of the second solution were mixed and stirred for about 10 min. The mixture was transferred to a heating mantle and refluxed for 45 min. The solution became green-black in the case of Ag. The color change was gradual in the case of Ag. Further refluxing of the solution resulted in the formation of a precipitate, which could be dispersed by sonication. The colloidal material was precipitated by the

addition of toluene. The precipitate was washed repeatedly with toluene and redissolved in 2-propanol. Dry powders were not redispersible (thus, the 2-propanol dispersions contained traces of toluene). The solutions (mother liquor as well as redispersed particles) were stable for over two months. In the present study, fresh colloidal Ag@TiO_2 dispersed in chloroform was prepared before each set of measurements. The stock solution was diluted with chloroform to obtain the desired concentrations of Ag@TiO_2 . No attempts were made to exclude the traces of 2-propanol (~0.4%) present in the colloidal Ag@TiO_2 and it was confirmed separately that the presence of 2-propanol did not affect the photochemical measurements.

The size of the Ag@TiO_2 core shell nanoparticles was also estimated from high resolution Transmission Electron Micrograph (TEM). The core (Ag) diameter varies in the range of 20–30 nm (Fig. 1(E)). The shell (TiO_2) thickness is 2–6 nm. The average diameter of Ag@TiO_2 nanoparticle is found to be <40 nm.

Preparation of Au Nanoparticles: Au nanoparticles were prepared using Lemongrass extract.³⁴ Tamarind leaf extract³⁵ and *Emblica officinalis* fruit extract³⁶ as natural source of reducing and capping biomolecules. Briefly, the broth used for the reduction of Au^{3+} ions to Au^0 was prepared by taking 50 g of thoroughly washed tamarind leaves as earlier reported by Ankamwar et al.³⁵ in a 500 mL Erlenmeyer flask with 200 mL of sterile distilled water; this mixture was then boiled for 5 min. 10 mL of this broth was added to 45 mL of 1×10^{-3} M aqueous chloroauric acid (HAuCl_4) solution at room temperature. The detailed synthesis of this nanoparticle is described elsewhere.³⁵ The size of the Au nanoparticles was estimated from High Resolution Transmission Electron Microscope (HRTEM) and also from Atomic Force Microscope (AFM). Figure 1(B) illustrates the HRTEM and AFM images of the synthesized single nanoparticle. From both the TEM and AFM images, it can be seen that Au nanoparticles are predominantly triangular in morphology. AFM analysis (surface profile analysis) of one single Au nanotriangle indicated that the particle has a thickness of 5 nm and edge length of 100 nm.

2.2. Spectroscopic Measurements

At the ambient temperature (296 K) steady state UV-vis electronic absorption and fluorescence emission spectra of dilute solutions (10^{-4} – 10^{-6} M) of the samples were recorded by using 1 cm path length rectangular quartz cells by means of an absorption spectrophotometer (Shimadzu UV-Vis 2101PC) and F-4500 fluorescence spectrophotometer (Hitachi), respectively. Fluorescence lifetimes were measured by using a Time-Correlated Single Photon Counting (TCSPC) method by using HORIBA JOBIN YVON FLUOROCUBE. The goodness of fit has been assessed with the help of statistical parameters χ^2

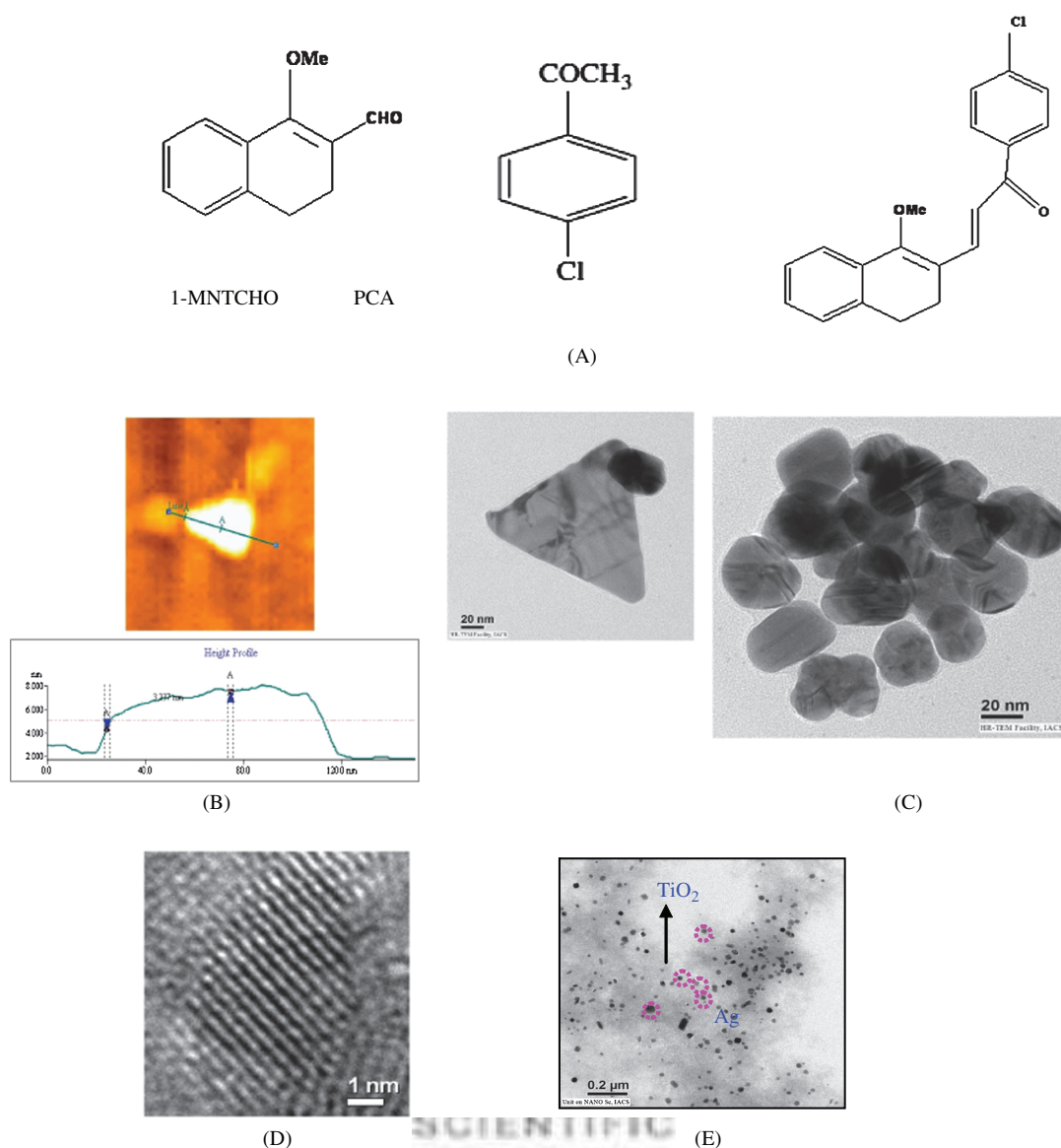


Fig. 1. (A) Molecular structure of the compounds MNCADH, PCA and 1 MNTCHO. (B) HRTEM micrograph of a single gold nanotriangle; AFM image of the biologically synthesized gold nanotriangle along with the surface height profile. (C) Representative TEM images of MK leaf extract-reduced silver nanoparticles. (D) HRTEM picture of a single TiO₂ nanoparticle. (E) TEM picture of Ag@TiO₂ core/shell nanoparticles.

and DW. All the solutions prepared for room temperature measurements were deoxygenated by purging with an argon gas stream for about 30 min. The size of the synthesized nanoparticles was estimated by using HRTEM (JEOL, Model JEM-2010). AFM image of Au nanoparticle was obtained using a multimode AFM (Veeco Metrology, Autoprobe diCP-II, Model No. AP0100) at ambient temperature with the help of silicon (Si) probes (RTESPA-M, Veeco, Santa Barbara, CA) in tapping (NC-AFM) mode. Long tips (aspect ratio 4:1) cantilever (Material: 1–10 Ω-cm phosphorous (n) doped Si) with spring constants ranging from 20 to 80 N/m and resonance frequencies of 245–285 kHz were used to image the surface morphology of the nanoparticle. Proscan Image Processing Programme (PIPP) software provided by the manufacturer

was used to measure the thickness and edge length of the Au nanoparticle.

2.3. Laser Flash Photolysis (LFP)

Nanosecond flash photolysis set-up (LFP) (Applied Photophysics) containing Nd:YAG (Lab series, Model Lab 150, Spectra physics) laser was used for the measurement of transient absorption spectra. The sample was excited at 355 nm (FWHM = 8 ns) laser light. Transients were monitored through absorption of light from a pulsed xenon lamp (250 W). The photomultiplier (IP28) output was fed into a Tektronix oscilloscope (TDS 3054B, 500 MHz, 5 Gs/s), and the data were transferred to a computer using the TekVISA software. The software Origin 6.0 was used for

curve fitting. The solid curves are obtained by connecting the points by using B-Spline option. The samples were deaerated by passing pure Argon gas stream for 30 min prior to each experiment. No degradation of the samples was observed during the experiment.

3. RESULTS AND DISCUSSION

3.1. UV-Vis Absorption and Steady State Fluorescence Emission Spectra in Different Solvents at the Ambient Temperature

UV-vis absorption spectra of the novel synthesized dyad MNCADH (Fig. 1(A)) have been recorded in various solvents including polar aprotic acetonitrile (ACN). It is apparent from the Figure 2 that in case of the dyad a new broad absorption band (λ_{abs} of peak position ~ 375 nm) is developed. This band is red shifted compared to the absorption bands of donor ($\lambda_{\text{abs}} \sim 317$ nm) and acceptor ($\lambda_{\text{abs}} \sim 249$ nm) measured in the same solvent ACN. Moreover, no broad red shifted band appears in the UV-vis spectra of the mixture of the free reactants (unlinked donor and acceptor). Instead the spectra show the superposition of the corresponding spectra of the donor and acceptor moieties. Further, from Figure 2 it appears that with increase of the polarity of the medium, the long wavelength absorption band of MNCADH at 375 nm suffers red shift indicating the charge transfer (CT) nature of 375 nm absorption band of the dyad.

When the CT absorption band is excited at 375 nm, a fluorescence emission spectrum of MNCADH peaking at about 490 nm is developed. Thus this band should be assigned as CT emission band. This proposition is also

confirmed from solvent effect studies. It is observed that with increasing the polarity of the solvents emission maximum of MNCADH at 490 nm clearly shifts towards red side, the shift being considerably larger than that observed in the solvent shifts of the absorption bands. This confirms the charge transfer nature of the fluorescence emission band produced due to the excitation of the ground state CT absorption spectrum.

From all the experimental measurements it is demonstrated that dyad MNCADH is dipolar in character and intramolecular charge separation occurs within the donor 1MNTCHO and acceptor PCA parts of the dyad MNCADH after photoexcitation of the ground state CT band.

As it was observed earlier by our research group,³⁷ similar isosteric systems exhibit primarily elongated i.e., *E*-type conformation in the ground state but upon photoexcitation extended conformation converts into the form of folded nature. The folded conformation facilitates the spatial overlapping of the orbitals of the donor and acceptor molecules which results in occurrence of energy destructive charge recombination process efficiently. In the case of the present dyad MNCADH also, NMR study shows the existence of only one conformer of trans nature, as evidenced from the value of the coupling constant, *J*. From the coupling constants of the olefinic protons (*J* = 15 Hz) it was inferred that the dyad present in the ground state is exclusively trans geometrical isomer or *E*-type (elongated nature).

From quantum chemical calculations at DFT level using Gaussian 03 software it was observed though the energy difference between trans and cis conformer is 4.7 Kcal/mole but the trans-cis interconversion energy barrier is found to be 64 Kcal/mol in ground state at the HF/6-31 g level. This ground state high energy barrier may be responsible for the hindrance of the trans-cis interconversion resulting in the formation of exclusively trans isomer only. This is actually observed from NMR study.

3.2. Time Resolved Fluorescence Measurements by TCSPC Method

Time resolved fluorescence measurements on the dyad clearly demonstrate the presence of two distinct species which might be due to the two different conformers: elongated (*E*-type) and folded (*Z*-type) nature. The best fit of the measured fluorescence decays exhibit the two different components, one around 1.7 ns and the other 0.025 ns (i.e., 25 ps order) (Table I). The interesting behavior is observed in presence of β -cyclodextrin (CD). It is apparent that with increase of CD concentrations (Table I) the fractional contribution associated with the longer component increases with the concomitant reduction of the corresponding parameter associated with the shorter ps species. As it is well known³⁸ that encapsulations of the dyad in

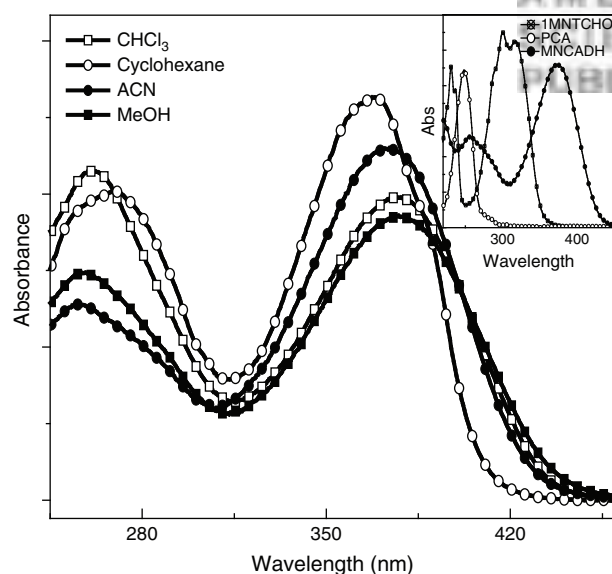


Fig. 2. Absorption spectra of MNCADH in different solvents. Inset: Absorption spectra of donor 1 MNTCHO, acceptor PCA and dyad MNCADH in ACN solvent.

Table I. Changes of fractional contributions (f_i) associated with fluorescence lifetimes of the different conformers (*E*- and *Z*-type) of the dyad in presence of CD and different noble metals, semiconductor nanoparticle TiO₂ and Ag@TiO₂ core/shell nanocomposite at the ambient temperature ($\lambda_{\text{exc}} \sim 375$ nm, $\lambda_{\text{em}} \sim 490$ nm).

Dyad MNCADH in different media	τ_1/ns	f_1	τ_2/ns	f_2	τ_{ip}^{**}	$k_{\text{CR}}(\text{S}^{-1}) (\sim 1/\tau_{\text{ip}})$
MeOH	1.78	0.11	0.025	0.89		
MeOH + 0.48 mM 'CD	1.77	0.19	0.023	0.81		
MeOH + 0.89 mM CD	1.80	0.25	0.027	0.75		
CHCl ₃	1.48	0.79	0.053	0.21	8 ms	0.13×10^3
CHCl ₃ + Au	1.53	0.74	0.049	0.26		
CHCl ₃ + Ag	1.19	1.0	—	—	33 ms	0.30×10^2
CHCl ₃ + TiO ₂	1.50	0.57	0.050	0.43		
CHCl ₃ + Ag@TiO ₂	1.42	0.64	0.053	0.36	11 ms	0.91×10^2

**The values (obtained from transient absorption decays) (see text) of ion-pair lifetime (τ_{ip}) and approximate rate of charge recombination processes $k_{\text{CR}} (\approx 1/\tau_{\text{ip}})$ for the dyad MNCADH in CHCl₃ and when combined with noble metal Ag nanoparticles and core/shell Ag@TiO₂ nanocomposite system.

CD cavity populate artificially the elongated conformation in the excited CT state due to inclusion complex formation, it appears that the longer component corresponds to the extended (*E*-) conformers whereas the shorter component having ps order should be due to folded or *Z*-type species.

3.3. Effect of Noble Metal Nanoparticles, Nano Semiconductor TiO₂ and Noble Metal-Semiconductor Nanocomposites on the Different Conformers, *E*- and *Z*-, of the Synthesized Photoswitchable Dyad

3.3.1. Steady State Fluorescence Measurements

Similar spectral behavior of the dyad i.e., gradual quenching of fluorescence intensity of MNCADH with increasing the concentrations of Au, Ag, TiO₂, Ag@TiO₂ core/shell nanoparticles has been observed. Figure 3 exhibits the lowering of emission intensity of MNCADH with addition of different concentrations of TiO₂. The above phenomena indicate that these nanoparticles when combine with

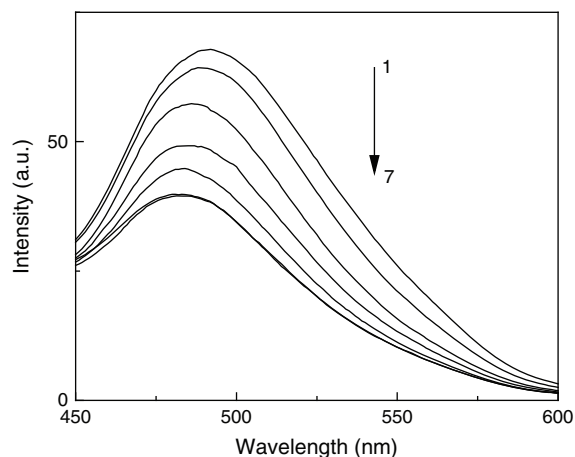


Fig. 3. Emission spectra of MNCADH after addition of different concentration of TiO₂ nanoparticles. (1) 0, (2) 5.6 mM, (3) 16.8 mM, (4) 27.8 mM, (5) 38 mM, (6) 0.058 M, (7) 0.08 M.

organic dyad system MNCADH form hybrid nanocomposite systems.

3.3.2. Time Resolved Fluorescence

From Table I it is apparent that if the nature of the solvent is changed from MeOH to non-hydrogen bonding solvent CHCl₃, the majority dyad species remaining in the excited state possess extended conformation (79%). Thus, even after photoexcitation, the photoswitchable dyad prefers to retain its elongated conformation in CHCl₃ environment. The situation was different when the surrounding medium was MeOH where folded conformational species in the excited state were found to dominate from time resolved studies. Thus the CHCl₃ appears to be much better medium relative to MeOH as the former medium hinders the formations of folded structure which facilitates the energy wasting and destructive charge recombination process. Further, in CHCl₃ medium when the dyad was combined with noble metal nanoparticles interesting observations were made. In case of Au nanoparticles, the percentage of the folded and extended conformations remain more-or-less same as they were in absence of this noble metal nanoparticles. When the other noble metal Ag is combined with the dyad, significant increase of extended conformations ($f_1 \sim 100\%$) indicates that this organic-inorganic nanocomposite may serve as a better light energy conversion devices relative to the device which could be built by replacing Ag with Au. It is known that folded conformation favors the energy wasting charge recombination process due to orbital overlapping of the two reactants (donor and acceptor) being relatively closer to each other.

The reverse situation from Ag nanocomposites was observed when the dyad is combined with semiconductor TiO₂ nanoparticles (Table I). For this composite system, the folded conformation grows significantly (f_2 increases) at the expense of the elongated conformational species (lowering of f_1) as it evidenced from the changes in the fractional contributions associated with the fluorescence

lifetimes of the two different species. The similar role of TiO₂ was also reported earlier by our research group in case of another photoswitchable dyad MNBA.³⁹ Thus the noble metal nanoparticles Ag and the semiconductor TiO₂ nanoparticles behave differently. However, when the dyad is combined with Ag (metal)-TiO₂ (semiconductor) core/shell nanocomposite system (Ag@TiO₂), the situation looks much better from only TiO₂ system. The concentrations of the folded species appear to be dropped down and become significantly smaller than that of the extended conformational species. Thus the presence of the metal Ag nanoparticles plays a constructive role in this core/shell nanocomposite in inhibiting energy destructive charge recombination process and upgrading the dyad-core/shell nanocomposite system to a better artificial light energy conversion device. The hybrid of Ag and organic dyad shows nearly 100% elongated conformations of the latter. This predicts the dyad when combined with the metal Ag, chance of charge recombination becomes very slim as majority contribution in emission originating from extended conformation where donor and acceptor being far apart suffer lack of overlapping with each other. The observation indicates the suitability for the construction of efficient light energy conversion devices taking especially Ag-dyad nanocomposite of all the systems studied in the present investigation.

3.3.3. Transient Absorption Spectra by Nanosecond Laser Flash Photolysis

The transient absorption decay profiles of the dyad were measured firstly in chloroform (Fig. 4) and then in mixtures of chloroform-Ag nanoparticles and chloroform-Ag@TiO₂ core/shell nanocomposites. The third

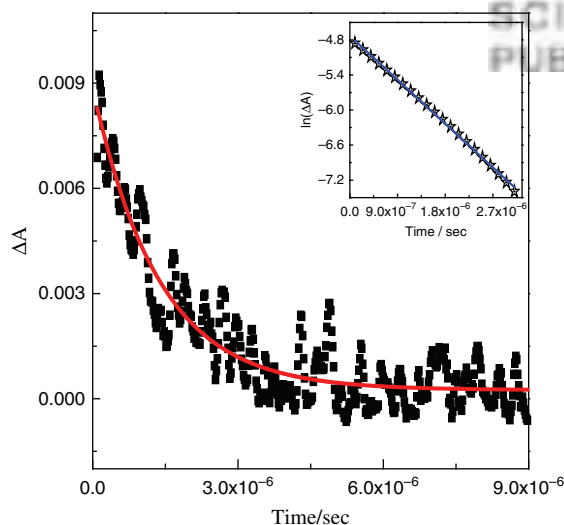


Fig. 4. Transient absorption decay profile of the dyad MNCADH when combined with noble metal Ag nanoparticles (Inset: plot of $\ln(\Delta A)$ as a function of delay times, obtained by subtracting the constant value of an absorbance at long delay time from the observed decay curve).

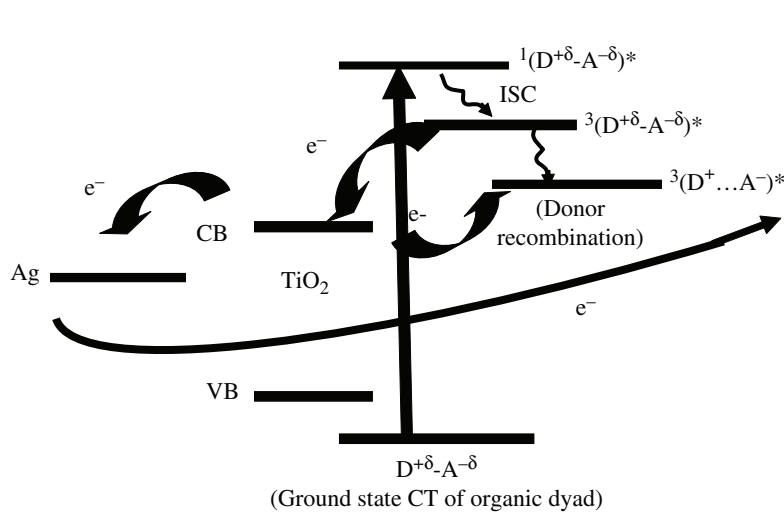
of Nd:YAG laser was used to excite the ground CT band of the dyad. It appears from the transient absorption decay profiles that the dyad when combined with the noble metal Ag nanoparticles, the ion-pair lifetime, τ_{ip} becomes significantly larger (~ 33 ms) than the situation when the former combines with Ag@TiO₂ core/shell nanocomposites (11 ms, Table I). Thus in presence of the noble metal Ag nanoparticles the survival duration of the charge-separated species within the dyad significantly increases. This observation appears to be due to the elongated conformation of the dyad which is largely dominating in this environment, as it is observed from the time resolved fluorescence studies discussed above. Thus, the energy destructive k_{CR} ($\sim 1/\tau_{ip}$) possesses slowest rate in case of the hybrid Ag-dyad nanocomposite system (Table I). It indicates the suitability for the construction of efficient light energy conversion devices especially with Ag-Dyad nanocomposite of all the systems studied here.

As the transient absorption decay profiles have been measured by using nanosecond laser flash photolysis techniques by using the delays in microsecond orders, it could be inferred that the excited singlet charge-separated species formed from the excitation of ground state CT complex relaxes to the corresponding triplet state by the intersystem crossing (isc) process. In the CT triplet level, further charge separations lead to the formations of charge-separated species whose level becomes further stabilized and closer to TiO₂ conduction band (Scheme 2). It appears that the partially charged donor, 1 MNTCHO, in CT triplet level, may prefer to donate electrons to the conduction band of TiO₂ rather than to the acceptor PCA. From energetic consideration this route for electron transfer appears to be possible. However, there is a possibility that from TiO₂ some electrons may return back to the triplet level of charge-separated species causing recombination with the donor cation. In Ag-dyad nanocomposite, due to the accumulation of the electrons in the much lower Fermi level of Ag, charge recombination process will be significantly impeded. This is probably the reason for the observed significant enhancement of the longevity of the charge-separated species within the dyad MNCADH when combined with noble metal Ag nanoparticles only.

In CHCl₃ medium the fluorescence lifetime of the free donor 1MNTCHO is determined to be 1.62 ns (τ_f) and the quenched lifetime of the donor when present in dyad is observed to be 1.18 ns (τ_q). The charge separation rate k_{CS} is estimated to be 2.3×10^8 s⁻¹ from the well known relation:

$$k_{CS} = 1/\tau_q - 1/\tau_f$$

In all the hybrid nanocomposite systems i.e., when the dyad is combined with noble metal/semiconductor systems, the charge-separation rates k_{CS} were found to be nearly the same order of magnitude ($\sim 10^8$ s⁻¹) and the charge recombination rates, as observed from transient absorption measurements by laser flash photolysis



Scheme 2. Pathways of charge separation and charge recombination within the dyad MNCADH and Ag@TiO₂ core/shell nanocomposite systems.

technique vary within 10^3 to 10^2 s⁻¹. The slowest charge recombination rate ($\sim 0.3 \times 10^2$ s⁻¹) was observed, as discussed above, for Ag-Dyad hybrid nanocomposite system. Thus all the systems studied here appear to be good candidates, from the appearance of faster charge-separation and much slower energy destructive charge recombination rates, for designing efficient light energy conversion devices. The suitability for the construction of efficient light energy conversion devices especially with Ag-dyad nanocomposite of all the systems studied here is apparent from the present investigation.

4. CONCLUSIONS

In this paper we have shown that organic dyad molecules could become potential light energy harvesting materials in the presence of nanocomposites. Though Ag@TiO₂ core/shell nanocomposite when combined with the dyad facilitates the conversions of majority Z-conformers of this dyad, present in the excited state, to E-type conformers, but the situation becomes more effective when the dyad combines with only noble metal Ag nanoparticles. Time resolved fluorescence studies indicate that in the hybrid of Ag-Dyad nanocomposite system nearly 100% elongated conformations persist even in the excited state. Among the nanocomposite systems studied in the present investigation, it appears from the transient absorption measurements that the dyad when combined with the noble metal Ag nanoparticles, the ion-pair lifetime, τ_{ip} becomes significantly large (~ 33 ms). This indicates the rate associated with energy destructive charge recombination processes k_{CR} ($\sim 1/\tau_{ip}$) is slowed down when the medium is changed from chloroform to the mixture of chloroform and Ag. Possibly due to the accumulation of the electrons in the much lower Fermi level of Ag, charge recombination process has been significantly impeded causing significant enhancement of the longevity of the charge-separated

species (~ 33 ms) within the dyad MNCADH. Ag-Dyad hybrid nanocomposite appears to be the best candidate amongst all the systems studied here for construction of efficient light energy conversion devices.

Acknowledgments: The authors thank Mr. Subrata Das of the Department of Spectroscopy for his active assistances in fluorescence lifetime measurements by time-correlated single photon counting technique. The authors express their gratitude to Professor Samita Basu of Saha Institute of Nuclear Physics, Salt lake, Kolkata for helping in the measurements of transient absorption spectra by using laser flash photolysis technique. BA expresses his appreciation to BCUD (BCUD/OSD/390; dated 16/11/2010), University of Pune for financial support. UKS acknowledges financial support from the project funded by the UGC, New Delhi (Grant No. PSW-038/10-11-ERO). TG specially thanks Department of Science and Technology (DST), New Delhi, India for Nano-Mission project (No: SR/NM/NS-51/2010) for supporting the various research work conducted in his photophysics and photochemistry group.

References and Notes

1. V. L. Colvin, M. C. Schlamp, and A. P. Alivisatos, *Nature* **370**, 354 (1994).
2. B. O Dabbousi, M. G. Bawendi, O. Onitsukaa, and M. F. Rubner, *Appl. Phys. Lett.* **66**, 1316 (1995).
3. N. Tessler, V. Medvedev, M. Kazes, S. Kan, and U. Banin, *Science* **295**, 1506 (2002).
4. T. Hasobe, S. Hattori, P. V. Kamat, Y. Wada, and S. Fukuzumi, *J. Mater. Chem.* **15**, 372 (2005).
5. R. A. J. Janssen and W. J. E. Beek, *J. Mater. Chem.* **14**, 2795 (2004).
6. H. S. Nalwa (ed.), *Handbook of Organic-Inorganic Hybrid Materials and Nanocomposites*, American Scientific Publishers, Stevenson Ranch, California (2003).
7. C. Sanchez, B. Lebeau, F. Chaput, and J. P. Boilot, *Adv. Mater.* **15**, 1969 (2003).
8. J. W. Kriesel and T. D. Tilley, *Adv. Mater.* **13**, 1645 (2001).

9. K. E. Gonsalves, L. Merhari, H. Wu, and Y. Hu, *Adv. Mater.* 13, 703 (2001).
10. E. Holder, N. Tessler, and A. L. Rogach, *J. Mater. Chem.* 18, 1064 (2008).
11. M. C. Scharber, D. Mühlbacher, M. Koppe, P. Denk, C. Waldlauf, A. J. Heeger, and C. J. Brabec, *Adv. Mater.* 18, 789 (2006).
12. C. Brabec, V. Dyakonov, and U. Scherf (eds.), *Organic Photovoltaics*, Wiley-VCH, Weinheim, Germany (2008).
13. T. Stöferle, U. Scherf, and R. F. Mahrt, *Nano Lett.* 9, 453 (2009).
14. (a) B. O'Regan and M. Grätzel, *Nature* 353, 737 (1991); (b) U. Bach, D. Lupo, P. Comte, J. E. Moser, F. Weissörtel, J. Salbeck, H. Spreitzer, and M. Grätzel, *Nature* 395, 583 (1998).
15. (a) R. A. J. Janssen and W. J. E. Beek, *Adv. Funct. Mater.* 12, 519 (2002); (b) V. L. Colvin, M. C. Schlamp, and A. P. Alivisatos, *Nature* 370, 354 (1994).
16. M. C. Schlamp, X. Peng, and A. P. Alivisatos, *J. Appl. Phys.* 82, 5837 (1997).
17. H. Mattoussi, L. H. Radzilowski, B. O. Dabbousi, E. L. Thomas, and M. G. Bawendi, *J. Appl. Phys.* 83, 7965 (1998).
18. W. U. Huynh, X. Peng, and A. P. Alivisatos, *Adv. Mater.* 11, 923 (1999).
19. D. C. Ginger and N. C. Geenham, *Phys. Rev. B* 59, 10622 (1999).
20. K. S. Narayan, A. G. Manoj, J. Nanda, and D. D. Sarma, *Appl. Phys. Lett.* 74, 871 (1999).
21. J. Lee, V. C. Sundar, M. G. Bawendi, and K. F. Jensen, *Adv. Mater.* 12, 1102 (2000).
22. (a) A. N. Shipway and I. Willner, *Chem. Commun.* 20, 2035 (2001); (b) A. Hagfeldt and M. Grätzel, *Acc. Chem. Res.* 33, 269 (2000).
23. M. Hilgendorff and V. Sundström, *J. Phys. Chem. B* 102, 10505 (1998).
24. J. Pan, G. Benkö, Y. Xu, T. Pascher, L. Sun, V. Sundström, T. Polivka, *J. Am. Chem. Soc.* 124, 13949 (2002).
25. M. Ritala, M. Leskelii, L. Niinistö, and P. Haussalo, *Chem. Mater.* 5, 1174 (1993).
26. V. M. Agronovich, G. C. La Rocca, and F. Bassani, *JETP Lett.* 66, 748 (1997).
27. G. Heliotis, G. Itskos, R. Murray, M. D. Dawson, I. M. Watson, and D. D. C. Bradley, *Adv. Mater.* 18, 334 (2006).
28. S. Blumstengel, S. Sadofev, C. Xu, J. Puls, and F. Henneberger, *Phys. Rev. Lett.* 97, 237401 (2006).
29. A. R. Clapp, I. L. Medintz, J. M. Mauro, B. R. Fisher, M. G. Bawendi, and H. Mattoussi, *J. Am. Chem. Soc.* 126, 301 (2004).
30. Q. Zhang, T. Atay, J. R. Tischler, M. S. Bradley, V. Bulovic', and A. V. Nurmikko, *Nat. Nanotechnol.* 2, 555 (2007).
31. (a) G. Mandal, S. Bhattacharya, and T. Ganguly, *J. Nanosci. Nanotechnol.* 10, 579 (2010); (b) G. Mandal, S. Bhattacharya, S. Das, and T. Ganguly, *J. Nanosci. Nanotechnol.* 12, 187 (2012).
32. K. Ohkubo, H. Kotani, J. Shao, Z. Ou, K. M. Kadish, G. Li, R. K. Pandey, M. Fujitsuka, O. Ito, H. Imahori, and S. Fukuzumi, *Angew. Chem. Int. Ed.* 43, 853 (2004).
33. B. Ankamwar, G. Mandal, U. K. Sur, and T. Ganguly, *Digest J. Nano Biostruc.* 7, 599 (2012).
34. S. Shiv Shankar, A. Rai, B. Ankamwar, A. Singh, A. Ahmad, and M. Sastry, *Nature Mater.* 3, 482 (2004).
35. B. Ankamwar, M. Chaudhary, and M. Sastry, *Syn. React. Inorg. Metal Org. Nano-Metal Chem.* 35, 19 (2005).
36. B. Ankamwar, C. Damle, A. Ahmad, and M. Sastry, *J. Nanosci. Nanotechnol.* 5, 1665 (2005).
37. M. Maiti, T. Misra, T. Bhattacharya, C. Basu, A. Dey, S. K. Sarkar, and T. Ganguly, *J. Photochem. Photobiol. A: Chemistry* 152, 41 (2002).
38. S. Bhattacharya, T. K. Pradhan, A. De, S. Roy Chaudhury, A. K. De, and T. Ganguly, *J. Phys. Chem. A* 110, 5665 (2006).
39. S. Bhattacharya, G. Mandal, J. Chowdhury, and T. Ganguly, *Chem. Phys. Letts.* 478, 215 (2009).

Received: 19 December 2011. Accepted: 19 March 2012.